

## Numerical simulation of 23 June 2016 Yancheng City EF4 tornadic supercell and analysis of lightning activity

GUO FengXia\*, LI Yang, HUANG ZhaoChu, WANG ManFei, ZENG FanHui,  
LIAN ChunHao & MU YiJun

*Key Laboratory of Meteorological Disaster, Ministry of Education (KLME), Joint International Research Laboratory of Climate and Environment Change (ILCEC), Collaborative Innovation Center on Forecast and Evaluation of Meteorological Disaster (CIC-FEMD), Key Laboratory for Aerosol-Cloud-Precipitation of China Meteorological Administration, Nanjing University of Information Science & Technology, Nanjing 210044, China*

Received March 2, 2017; accepted September 1, 2017; published online November 2, 2017

**Abstract** Based on the Weather Research Forecasting (WRF) model that features charging and discharging parameterization, relationships between tornado, hail and lightning were investigated for a tornado-producing (EF4 intensity) supercell thunderstorm over Yancheng City in Jiangsu Province, China, on 23 June 2016. Based on a sounding at 0800, there was a low lifting condensation level, substantial convective available potential energy (CAPE), and strong vertical wind shear near Yancheng City, which promote supercell development. At 1400, observations revealed that hail production and a dramatic increase of positive cloud-to-ground flash rates occurred simultaneously, maximizing five minutes later. The tornado occurred 30 min after the hail production. The time of minimum positive cloud-to-ground flash rates was 15 min later. The simulation indicated that the tornadic supercell moved eastward and that positive cloud-to-ground flash rates increased dramatically at 1400, the same as observed, but their maximum was 5 min later than observed. The simulated updraft volume peaked at 1425 and the simulated downdraft volume maximized 5 min later, when the mesocyclone formed. Simulated reflectivities showed no hook echo and horizontal winds for different height at mid-low levels had a different cyclonic shear at 1430, favorable to mesocyclone formation. Based on the simulated results, the region of positively charged graupel ascended resulting from the region of high liquid water content was lifted by the strong updraft, forming a mid-level strong positive charge region. A lower negative charge region formed by the inductive charging mechanism of collisions between graupel and droplets at the bottom of the cloud, conducive to positive cloud-to-ground flashes.

**Keywords** Tornado, Supercell, WRF, Hail, Positive cloud-to-ground flashes

**Citation:** Guo F X, Li Y, Huang Z C, Wang M F, Zeng F H, Lian C H, Mu Y J. 2017. Numerical simulation of 23 June 2016 Yancheng City EF4 tornadic supercell and analysis of lightning activity. *Science China Earth Sciences*, 60: 2204–2213, doi: 10.1007/s11430-017-9109-8

### 1. Introduction

An EF4-intensity tornado occurred in Yancheng City, Funing County, northern Jiangsu Province, China about 1430 LST (Local Standard Time; all subsequent times LST) on 23 June 2016. A majority of farmhouses, factories and schools collapsed or had their roofs torn away. Traffic jam happened,

roads were destroyed, and water and electricity supply installations were damaged. As of 26 June, the tornado had caused 99 deaths and 800 injuries. A tornado of such intensity is rare in Jiangsu Province, with the last one occurring in 1979. Over recent decades, tornadoes have repeatedly affected Yancheng City, with a particularly strong one leading to direct economic losses of over a hundred million yuan in 20 April 2005. Just four days later, there was a severe tornado with hail in the city again, causing 13 deaths, 825 injuries, and economic losses in excess of 14.2 billion yuan.

\* Corresponding author (email: guofx@nuist.edu.cn)

A tornado with measured wind speed perhaps  $140 \text{ m s}^{-1}$  and averaging  $\sim 100 \text{ m}$  in diameter is defined as a violently rotating, narrow column of air. Tornadoes affect small areas but are very destructive. Fujita developed an F0–F5 damage scale based on the degree of damage relative to wind speed (Fujita, 1971). The National Oceanic and Atmospheric Administration reclassified the F-scale as EF0–EF5 in 2007.

Tornadoes occur in many parts of the world. Two of the greatest concentrations of tornadoes outside the United States with the most frequency are found in Argentina and Bangladesh (<https://www.nssl.noaa.gov/education/srvwx101/tornadoes>). The spatial maximum in tornado occurrence over the Great Plains extends from western Texas into eastern Colorado, Nebraska, and Iowa (Brooks et al., 2003). Dry and cold air from the Rocky Mountains meets warm and humid air from the Gulf Coast in spring, generating strong environmental wind shear, lifting, and moisture, favoring tornadic supercell development (Carlson et al., 1983; Kelly et al., 1978). About 1000–2000 tornadoes strike the U.S. yearly, mainly east of a line from Nebraska to Texas, marking the boundary of the Great Plains. The tornado frequency in China is much lower than the U.S.. Generally, there are larger numbers of tornadoes in plains areas such as Jianghuai, the Lianghu Plain, South China, Northeast Plain, and southeastern North China Plain (Yao et al., 2015). Jiangsu Province has the one of the greatest concentrations. This province is largely composed of plains with many rivers and lakes; its plain accounts for  $>70\%$  of the total area, the largest proportion in China. Yancheng City is in the northern part of the province, on a plain with elevation  $<10 \text{ m}$ , with the most extensive water area in the province. Yao et al. (2015) found that more than 80% over tornadoes were in eastern China, and these were strongly related to terrain elevation. Most tornadoes occur over plains than over hilly regions. Jiangsu Province is on a plain with abundant water vapor, which is conducive to severe convective weather. There were 1070 tornadoes in the province from 1956 to 2010 (Pan, 2008), with most occurring on summer afternoons. There were nine EF3 and 28 EF2 tornadoes in the province over 1961–2010 (Fan and Yu, 2015). The area of greatest frequency of violent tornadoes in the province includes the cities of Nantong, Yancheng and Taizhou (Yao et al., 2015).

The most destructive tornadoes are produced by supercells. Davies-Jones presented observations and simulations demonstrating that tornadic supercells have three stages. First, the updraft begins rotating and a mesocyclone forms aloft. Next, a narrower vortex develops near the surface (thus forming a rotating column that extends from the ground to upper levels). Finally, a tornado develops from contraction of the near-surface cyclone (Davies-Jones, 2015). However, tornado formation is not fully understood. Supercells require adequate water vapor, energy from instability, rising air, and especially, strong vertical wind shear (Weisman and Klemp, 1984).

To research characteristics of the Yancheng EF4 tornado of 23 June 2016, the synoptic background prior to tornado production was analyzed, and addressed the relationships between the tornado, hail and lightning using Weather Research Forecasting (WRF) model. This model features a charging and discharging parameterization scheme.

## 2. Synoptic conditions and model introduction

### 2.1 Synoptic conditions

On 23 June 2016, the area along the Yellow and Huaihe Rivers had high temperature and humidity. At the 500 hPa level, there were cold vortices, and a trough to their east at mid-low levels (700 and 850 hPa). There were surface cyclones and cold air to their rear (figure not shown). There was southwesterly jet flow at lower levels and a northwest jet at mid-upper levels, giving strong wind shear in the vertical.

From a sounding at 0800 in Sheyang County, convective available potential energy (CAPE) and the lifting condensation level (LCL) were  $495.59 \text{ J kg}^{-1}$  and  $976.1 \text{ m}$ , respectively. Horizontal wind speed gradually increased with height with clockwise turning, which is favorable to severe convective weather (Figure 1) (Houze et al., 1990; Zheng et al., 2009; Moller et al., 1994). Based on Nation Centers for Environmental Prediction (NCEP) FNL 6-hour reanalysis data, the CAPE and LCL were  $1600 \text{ J kg}^{-1}$  and  $\sim 390 \text{ m}$ , respectively. There was horizontal wind with clockwise shear over Yancheng, satisfying criteria of Moller et al. (1990) that show that moderate-strong CAPE, a low LCL, and strong vertical

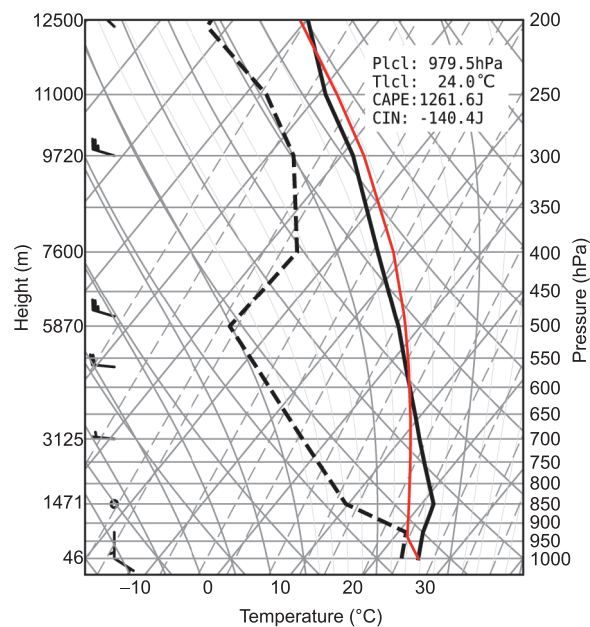


**Figure 1** T- $\ln P$  plot at 0800LST 23 June 2016 in Sheyang County, Yancheng City, Jiangsu Province.

wind shear are beneficial to the occurrence of high-precipitation supercells at mid-latitudes. The low LCL and substantial CAPE provide sufficient energy for supercells and, in particular, the strong vertical wind shear is favorable for their growth and organization.

At 1300, an eastward-moving supercell was over Huai'an City, associated with strong convergence at the surface. This resulted in localized severe convective weather, i.e., strong winds and hail in Sheyang and Funing counties. About 1430, EF4 tornado occurred at the border of Lianshui and Funing counties.

## 2.2 Model introduction

The three-dimensional compressible, nonhydrostatic WRF model (version 3.3.1) employs the two-moment, 6-class bulk microphysical scheme. The six bulk species are rain, cloud water, cloud ice, snow, graupel, and hail. Inductive charge separation and five parameterizations of non-inductive charge separation have been implemented in WRF (Fierro et al., 2013). The simulation domain (Figure 2) consists of a parent domain (d01) with inner (d02) and innermost (d03) nests, with horizontal resolutions 9, 3, and 1 km, respectively. Corresponding horizontal grid dimensions were  $181 \times 151$ ,  $364 \times 364$ , and  $553 \times 493$ , with time steps set to 45, 15 and 5 s. The stretched vertical grid had 60 levels with domain top set at 50 hPa ( $\sim 20$  km). The NCEP FNL 6-hourly reanalysis data for an 18-h period starting at 1800 on 22 June 2016 were used as initial boundary conditions.

Shortwave and longwave radiation were both represented by the Rapid Radiative Transfer Model (RRTM). The surface layer, land surface and planetary boundary layer schemes

and cumulus parameterization used the Monin-Obukhov with Carslon-Boland scheme, Noah Land Surface Model, Yonsei University scheme, and Kain-Fritsch scheme, respectively (the grid resolutions of d02 and d03 were used to better resolve the development of convection, and only d01 had cumulus parameterization). The inductive charging rebounding collision involving graupel-droplet collision (Brooks and Saunders, 1994) and non-inductive charging rebounding collisions involving graupel/hail and snow/cloud ice are documented by Brooks and Saunders (1994) and Saunders and Peck (1998), respectively (or in Mansell et al., 2005). The microphysics process has detailed Appendix in Mansell et al. (2010). Mansell et al. (2005) demonstrated the charging behavior from parameterizations of five non-inductive charging laboratory studies in the context of a numerical storm simulation. The results showed that the two schemes based on rime accretion rate are more sensitive to the microphysical conditions, and they appear also to be more versatile in the possible charge structures they can produce. The second RAR-based (riming accretion rate) scheme (SP98) is from Saunders and Peck (1998). Fierro et al. (2013) used SP98 scheme in WRF model to simulate a continental squall line and a tropical cyclone. Overall, the simulated spatial flash pattern for both cases exhibited reasonable agreement with observations. For the tropical cyclone, the simulated gross charge structure was in accord with observations. The simulated flash extent density for both cases were also evaluated against those obtained with the recently developed McCaul et al. (2009) diagnostic lightning prediction schemes and exhibited overall good agreement with each other. As discussed above, SP98 is chosen in our simulation.

The discharging parameterization proposed by MacGor-

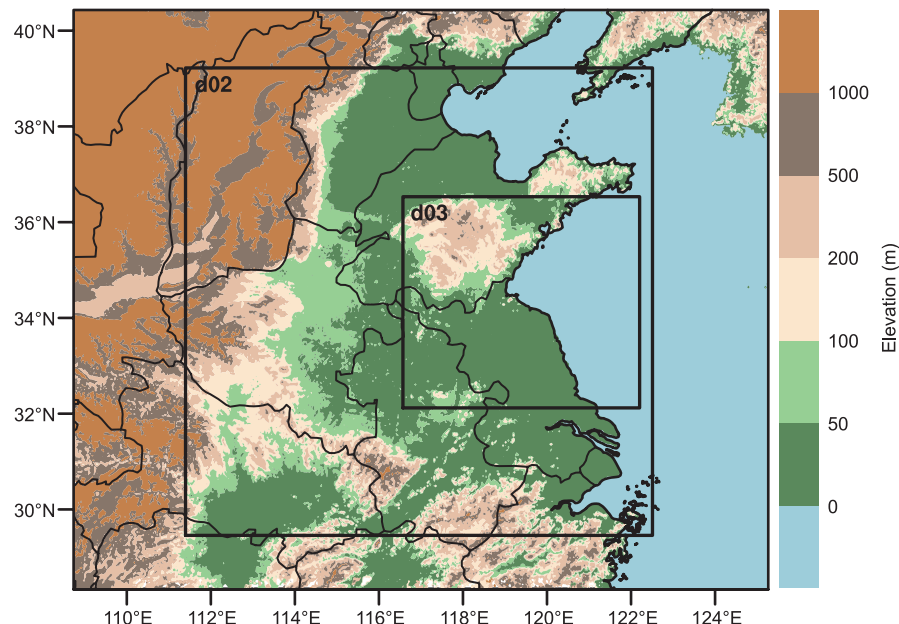


**Figure 2** Simulation domain and the distribution of elevation (d01, d02 and d03 is parent domain, inner nest and inmost nest, respectively).

man et al. (2001), which simulated intracloud (IC) and cloud-to-ground (CG, including positive and negative, i.e., +CG and -CG) flashes, was also used.

### 3. Simulation results

#### 3.1 Detailed supercell evolution

Simulated and observed reflectivity is exhibited in Figures 3 and 4, respectively. Figures 3a and 4a indicates that the supercell was in the developing phase at 1300, owing to weak reflectivity. The supercell eastwardly moved and will step into the mature phase at 1330 in Figure 3b, the same tendency as

well as shown in Figure 4b. At 1400, the supercell under the mature phase same as the observed base on the reflectivity in Figure 4c, but the new cell occurred in the northwest of the supercell, however, the new cell, which weaker than the observed, occurred in the north of the supercell. The simulated reflectivities at the storm center were >60 dBZ, but observed <60 dBZ and >50 dBZ (Figures 3c and 4c). The significant hook echo exhibited in Figure 4d and the EF4 tornado had occurred based on the report, and Figure 3d demonstrate that the supercell had reached the most sever phase, with the reflectivities >70 dBZ at the center, but no significant hook echo. The duration for tornado is about 30 min, and the supercell had went the declining phase as time went on (Figures 3e and

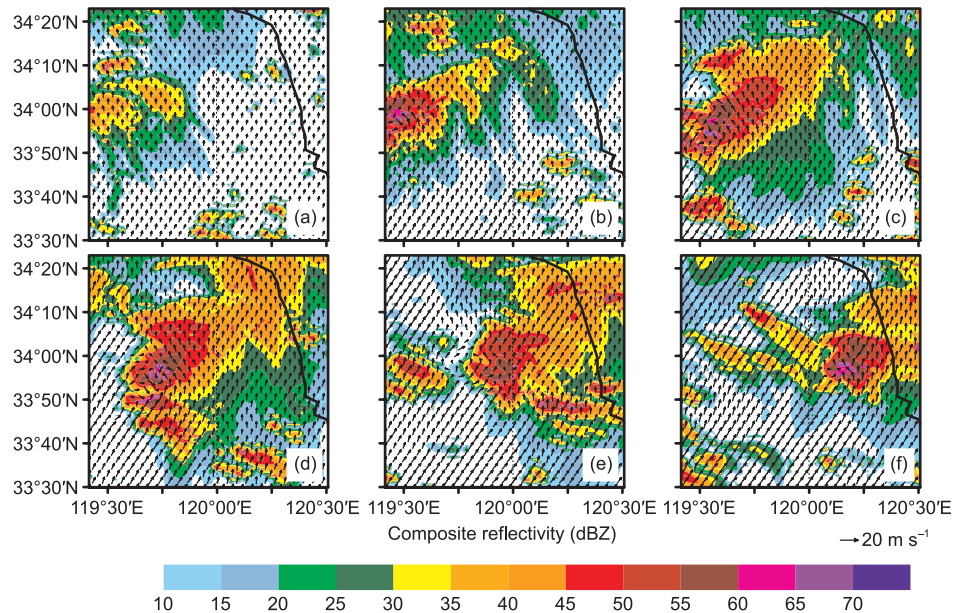


**Figure 3** Simulated composite reflectivity and horizontal wind at 700 m. (a) 1300; (b) 1330; (c) 1400; (d) 1430; (e) 1500; (f) 1530.

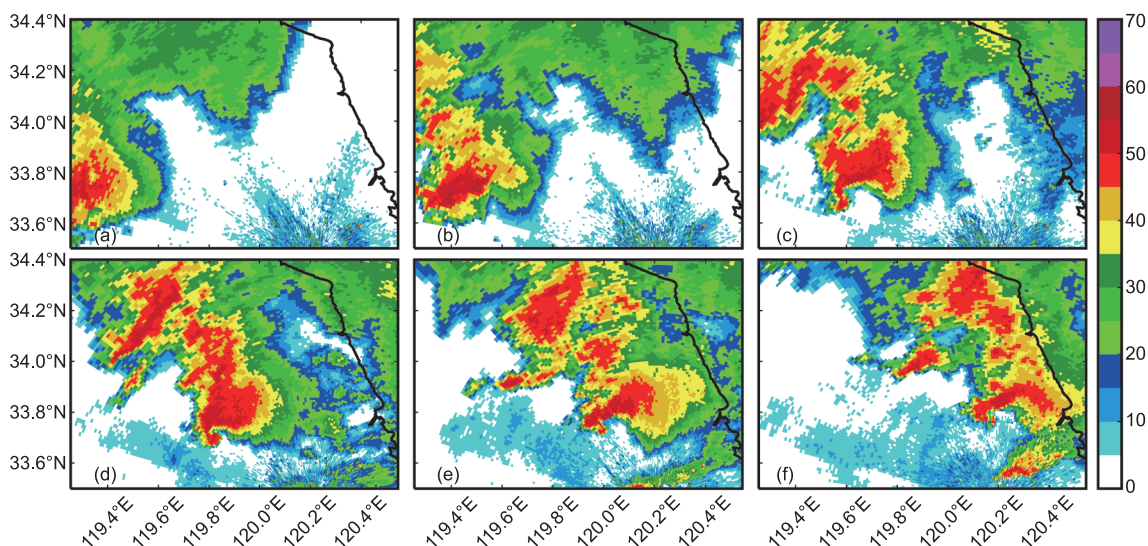


**Figure 4** Observed radar reflectivity at the 0.5° elevation of Yancheng S-band radar. (a) 1300; (b) 1328; (c) 1402; (d) 1431; (e) 1459; (f) 1528. The black arrow points to the hook echo in (d).

4e), and the simulated supercell splits out a small area of strong reflectivity that southeasterly moved.

The simulated result demonstrates that the intensity of cyclonic shear of the horizontal wind had strengthened (Figure 3d) and the maximum horizontal wind and downdraft were 56.4 and 15 m s<sup>-1</sup>, respectively. Lower-level warm and humid air was lifted by the combined effect of a near-surface pool of cold air (caused by strong downdrafts) and the vertical wind shear. This strengthened the supercell and extended its lifetime. Downdrafts are required for tornadogenesis when there is preexisting rotation near the surface, and the rear-flank downdraft is crucial to tornadogenesis (Davies-Jones, 1982a, 1982b). However, the dynamic relationship between that downdraft and tornadogenesis remains poorly understood (Markowski, 2002; Wicker and Wilhelmson, 1995). At 1500, the supercell had weakened, and rear-flank horizontal winds continued to have weak cyclonic shear. A new cell appeared in the right front of the supercell and gradually intensified. The storm center strengthened again, owing to merger of that

cell with the supercell, but the horizontal winds did not show cyclonic shear at 1530.

Under the simulated result, the horizontal wind was from the south and southwest at the 700 m and 3 km levels, respectively, demonstrating vertical wind shear. This was favorable to growth of the supercell. As the storm continuously intensified, cyclonic shear appeared at lower levels, supporting formation of a mesocyclone. The obvious inflow notch displays in Figure 5a, which maintain the persistent updraft. Figure 5b shows a clear weak echo region (WER) above the inflow at low levels, indicating a strong updraft. The observed and simulated echo top ( $\geq 50$  dBZ) both are about 10 km (Figure 5b and c). Figure 5c demonstrated WER exist in resulting from strong updraft. The distribution of simulated vertical-cross reflectivity is consistent with the observed, but the echo strength is larger than observed from Figure 5b and 5c. The area of the reflectivities great than 50 dBZ extended above the  $-20^{\circ}\text{C}$  level, favoring hail production (Witt et al., 1988).

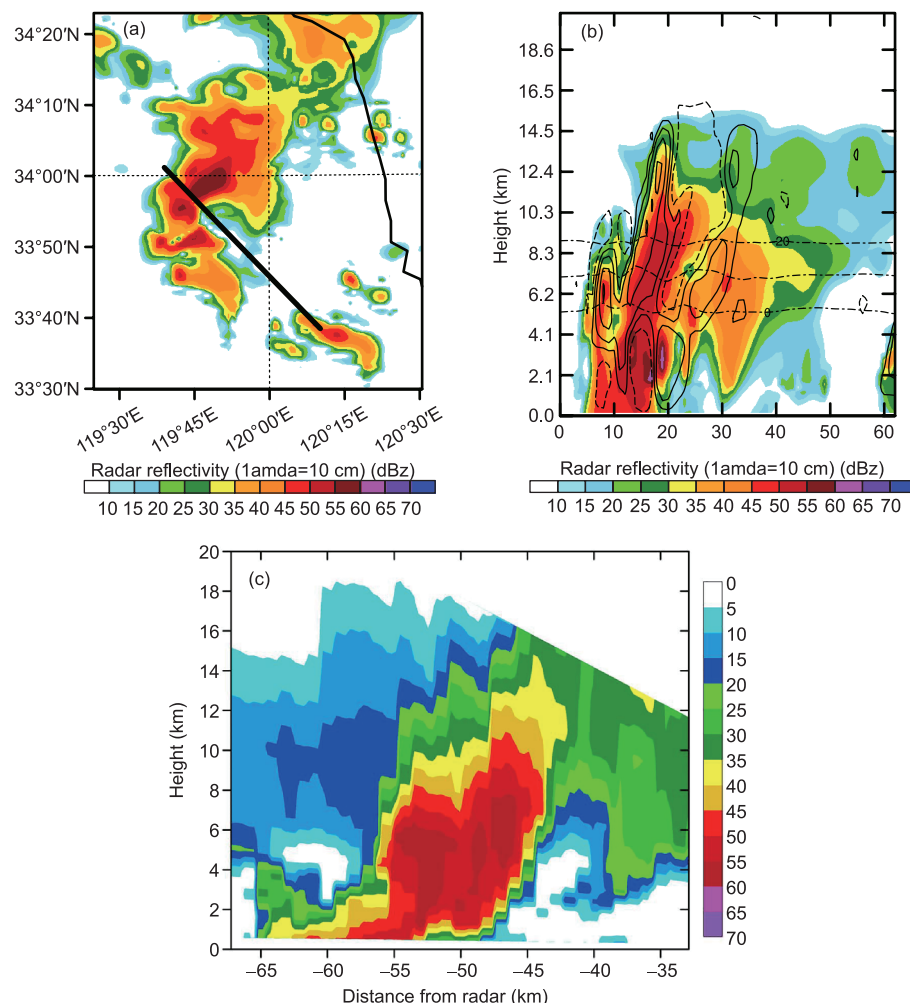


**Figure 5** (a) The contour of reflectivity and (b) vertical-across plot for reflectivity along the black line, the black solid and dash line means updraft ( $2, 5, 10, 15 \text{ m s}^{-1}$ ) and downdraft ( $-5, -1 \text{ m s}^{-1}$ ), respectively, at 1435. The black dot dash line means temperature ( $0, -10, -20^{\circ}\text{C}$ ). (c) Observed vertical-cross plot for reflectivity.

### 3.2 Relationship between hail and ground flashes

The lightning detection network of China Meteorological Administration (CMA) can detect positive and negative cloud-to-ground flashes through detecting the wideband VLF/LF (Very Low Frequency/Low Frequency) electric field signature of lightning discharges. Lightning location sensors included in it combine the proven accuracy of Magnetic Direction Finding (MDF) technology with the benefits of Time-of-Arrival (TOA) technology to achieve greater location accuracy and detection efficiency than either technology can produce alone. The lightning detection network indicated a dominance of +CG flashes 124 +CGs and 75 -CGs and simulated 139 +CGs, no -CGs, and 2304 ICs over the period 1330 to 1500. Figure 6 demonstrates that the -CG flash rate maximized at 1330, with few +CG. At 1400, these rates decreased to zero and there was hail. +CG flash rate sharply increased, reaching a maximum ( $4.8 \text{ fl min}^{-1}$ ) 10 min later, followed by a slow decrease. The supercell had predominantly positive ground flashes for at least 30 min. -CG flash rate increased over a period of increased +CG flash rate. Both +CG and -CG flash rates peaked simultaneously and then rapidly decreased. The tendency of -CG flash rates was similar to that of +CGs but with smaller values in general ( $\leq 1 \text{ fl min}^{-1}$ ). All simulated CGs were +CG, with few +CGs from 1300 to 1330. +CG flash rates increased from 1300 to 1400, when there was hail. The decreasing tendency of observed +CG flash rates was consistent with the simulation from 1400 to 1445.

Simulated IC flashes began at ~1245 and then quickly increased. The time of ground flash maxima agreed between observed and simulated. The updraft volume increased when IC and CG flash rates increased simultaneously, peaking at nearly the same time. The downdraft volume also increased before IC and CG flash rates peaked; 10 min later, the updraft

volume maximized (Figure 7). Some research has indicated that many thunderstorms have predominantly +CG and few -CG flashes, a result of increased updraft strength, hail, and updraft extent. Frequent +CG flashes began nearly simultaneously with dramatic increases in storm updraft and hail production. Only a few supercell have predominantly -CG activity (Curran and Rust, 1992; Branick and Doswell, 1992; Lang and Rutledge, 2002; Wines et al., 2005), which is consistent with the results of the work.

At 1400, hail production and the height of the reflectivity core decreased, corresponding to the downdraft and reflectivities  $> 60 \text{ dBZ}$  (Figure 8a). This demonstrated that hail was falling. The charge structure exhibited an inverted tripole charge structure (Figure 8b) consisting of a main positive charge region with greater charge density at  $-10^\circ\text{C} < T < -5^\circ\text{C}$  and an upper negative charge region and a lower negative charge region at about  $0^\circ\text{C}$  in the strong updraft. A region of weak echo at the side of strong echo region had weak updrafts. It can be seen from the distribution characteristic of strong echo. The weak echo volume was at the dissipating stage of convection. In the weak echo volume, there was a quasitripole charge structure with a very large LPCC (lower positive charge center) compared with the typical tripole charge structure. Each charge region was small and density was weak. The LPCC nearly touched the ground due to precipitation seen from the height of strong echo.

In Figure 9, the graupel mixing ratio is much larger at the strong updraft, but the ice mixing ratio is smaller. The charge region of graupel and ice is coincident with the maximum graupel mixing ratio. We used the non-inductive charging parameterization proposed by Saunders and Peck (1998). The graupel had positive charge and the ice negative, owing to non-inductive, graupel-ice charge separation. The rime accretion rate RAR ( $= EW \times V$ , where  $EW$  and  $V$  are the effective cloud water content and the relative velocity of between

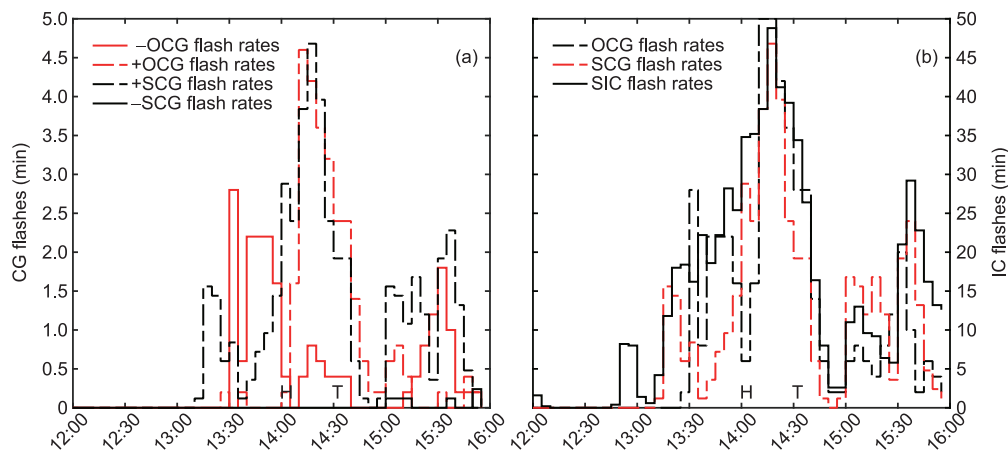


**Figure 6** Time series plots of (a) observed and simulated the rate of +/-CG (b) observed the rate of CG and simulated the rate of CG and IC for a period from 1200 to 1600 within 50 km of the tornado center in the supercell. +/-OCG means that observed positive/negative ground flashes, +/-SCG means simulated positive/negative ground flashes, OCG and SCG means observed and simulated total CG. The black letters H and T means the time of hail production and tornado, respectively.

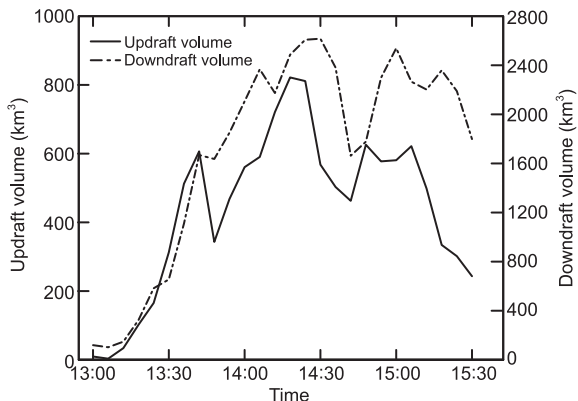


**Figure 7** Time series plots of updraft volume ( $\text{updraft} \geq 10 \text{ m s}^{-1}$ ) and downdraft volume ( $\text{downdraft} \leq -3 \text{ m s}^{-1}$ ).

colliding particles, respectively) was greater than the critical RAR, and vice versa. The region of graupel with positive charge enlarged and extended upward, so the large region of high RAR caused by substantial liquid water reached greater heights because of strong updrafts and the region of high cloud water content ascended. This caused the strong positive charge to appear in the severe convective region, a result of the region of graupel with positive charge expanding and extending upward. The low-level regions of negative charge were mainly caused by negatively charged graupel, under the influence of inductive graupel-droplet charge separation (figure not shown). +CG flashes in the model required a lower negative charge region for initiation (Wines et al., 2005; Gilmore and Wicker, 2002; Guo et al., 2016; Tan et al., 2016). The simulation also showed the frequent +CG trigger zone between the regions of lower negative charge and

mainly positive charge resulting from the greater potential between the lower negative charge region with weaker charge density and upper positive charge region. Several hypotheses, including inverted dipole or inverted tripole charge structures, have been put forward to explain the charge structure leading to +CGs, as reviewed by Williams (2001). Most observations confirm the existence of an inverted polarity charge structure (Zhang et al., 2001; MacGorman et al., 2005; Rust et al., 2005). There is frequent IC flash initiation between the region of mainly positive charge and that of upper negative charge, but the height of ICs is higher than in typical thunderstorms. The lower region of negative charge does not discharge to the ground because of no positive charge below; moreover, the height of the upper region of negative charge is greater, which also does not discharge. There were few -CG flashes between 1400 and 1440, i.e., from hail production to tornado occurrence 10 min later.

Severe convective activity and each charge region maintained high elevations after hail production, and the charge structure was dominated by an inverted tripole charge structure that generated frequent +CG flashes. Nonetheless, +CG and IC rates greatly decreased over the period of hail and enhanced downdrafts.

Analysis of radar reflectivity in excess of 60 dBZ by Gilmore and Wicker (2002) showed that frequent +CG flashes are strongly correlated with the descending core of solid precipitation. Reap and MacGorman (1989) found that such flashes are always coincident with hail production. This is consistent with the present results, which show that the time of frequent +CG flashes was when the convection was much stronger in the severe thunderstorms, with frequent IC

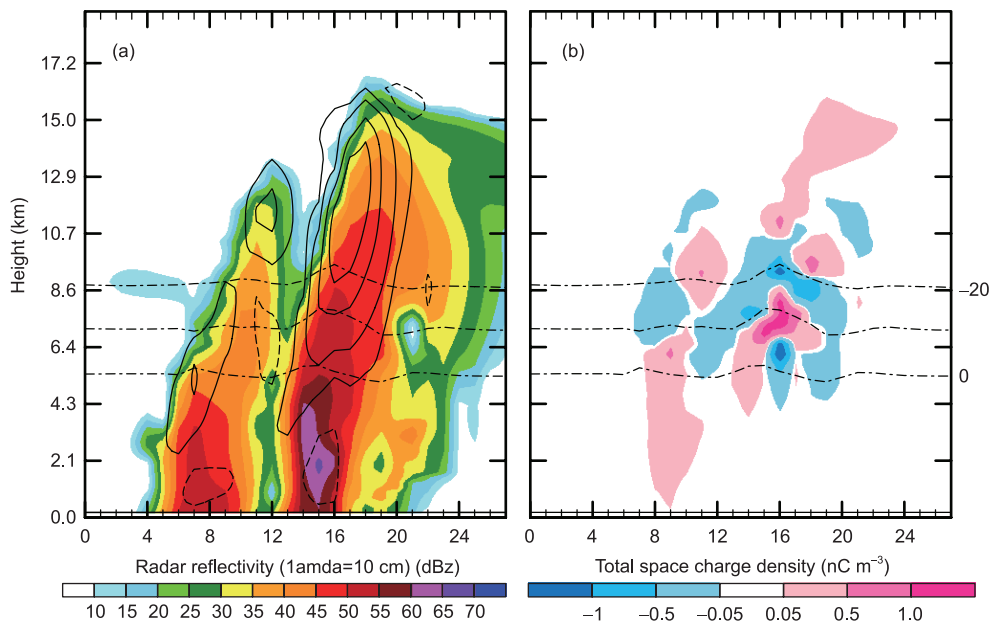


**Figure 8** The vertical-cross plot of reflectivity at 1400, the black solid/dash line means updraft ( $2, 5, 10, 15 \text{ m s}^{-1}$ )/downdraft ( $-5, -1 \text{ m s}^{-1}$ ) (a). The distribution of space charge, the black dot dash line means temperature ( $0, -10, -20^\circ\text{C}$ ) (b).

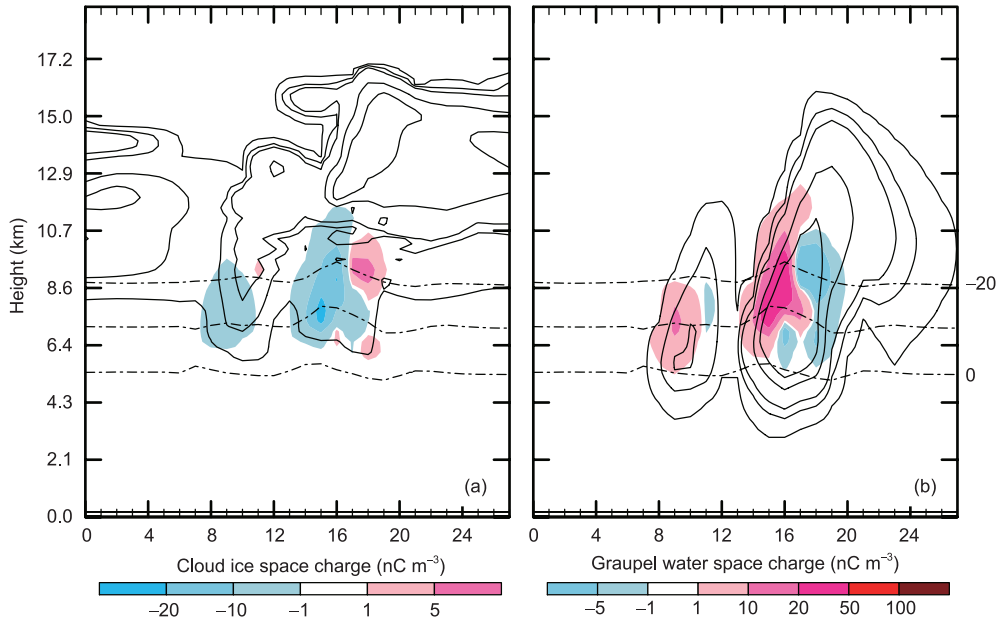


**Figure 9** The charge distribution and mixing ratio of ice (a) and graupel (b), the black solid line means the mixing ratio of ice ( $0.01, 0.05, 0.1, 0.5, 1, 1.5 \text{ g kg}^{-1}$ )/graupel ( $0.1, 0.5, 1, 3, 5 \text{ g kg}^{-1}$ ) in (a)/(b), the black dot dash line means temperature ( $0, -10, -20^\circ\text{C}$ ).

flashes and hail. Therefore, frequent +CG flashes demonstrate that such severe thunderstorms produce disastrous weather phenomena.

### 3.3 Relationship between tornado and ground flashes

Figure 6 demonstrates that the observed and simulated results both reveal a substantial increase in the rate of +CG flash from zero to the peak, and the tornado, which formed 10–15 min after the maximum +CG flash rate, occurred prior to the minimum rate of CG flash. The tendency of observed –CG flash rate was consistent with that of observed +CG flash rate, but lower than +CG flash rate, from hail-produce to tornado formation (Figure 6a). During the period, the tendency of simulated +CG flash rate was in accord with that of observed +CG flash rate, and with nearly same value, but the simulated –CG is 0 (Figure 6a). As shown in Figure 6b, the rate of observed and simulated ground flashes at tornado formation was  $3 \text{ and } 2 \text{ fl min}^{-1}$ , respectively, but this rate gradually decreased during the tornado duration. During that period, the rate of IC flash also steadily declined, with a minimum 20 min after tornado formation. The ground and cloud flashes activity were enhanced after hail-produce, but decrease prior to tornado formation. This dropping may result from the lower charge region was elevated by strong updraft.

Ice particles concentrate at mid-low levels because of strong updrafts and warm and humid air ascending to upper levels during the developing phase. This prolongs the collision-coalescence process of particles and allows sufficient time for the storm to produce an ample supply of embryonic particles for graupel and hail production. Then, downdrafts are enhanced by the descent of large particles

(e.g., hailstones). Figure 7 shows that the updraft volume peaked before tornado occurrence 10 min later. The downdraft volume maximized at the time of tornado formation, which demonstrates that the tornado requires strong updrafts and downdrafts. The downdraft volume increased again at 1500, but the tornado was not invigorated because of strong downdrafts causing divergence near the surface weakened vorticity. Moreover, the updraft produced by helical lifting of boundary-layer air had no concentrated low-level source of vorticity with which to connect. The weaker updraft could not maintain the persistent rotating updraft.

## 4. Discussion

Most of supercell dominate by +CG flashes, and produce tornado and severe hail (Browning, 1977). The relationship between tornadoes and ground flashes has previously documented from tornadic supercell. MacGorman et al. (1985) and Kane (1991) found that tornadoes occurred after ground flash rates had begun a decrease from peak values, but prior to reaching a local minimum. In 20 of these tornadic storms, the tornado touchdown time coincided with the decrease in ground flash rate. MacGorman and Burgess (1994) believed that tornadoes were usually produced when ground flash rates were either  $< 0.5 \text{ min}^{-1}$  or near a local minimum, and in their study of 15 storms, they reported that the most violent tornado produced by a storm always occurred after the maximum positive ground flash rate, whenever that maximum was at least 1.5 flashes per minute. Figure 5 shows that tornado occurred prior to the local minimum (observed and simulated both less than  $0.5 \text{ min}^{-1}$ ) for ground or +CG flashes.

The strongest tornadoes usually occurred after the rate

of ground flashes peaked (MacGorman and Burgess, 1994; Bluestein and MacGorman, 1998). Perez et al. (1997) analyzed 42 severe tornadoes (F4 and F5) in tornadic supercells, finding that the rate of ground flashes peaked prior to tornado formation in 32 of the 42 cases. Besides, MacGorman et al (1989) noted that ground flash rate increase after the tornado dissipate in two tornadic storms, and MacGorman and Nielsen (1991), Kane (1991) documented ground flash rate reach peak duration of tornadoes. The ground flashes increased when tornado was occurring in some storms (MacGorman and Burgess, 1994). The variety for relationship between tornado and CG was demonstrated from above documented researches.

Some thunderstorms dominated +CG activity duration at least 30 min tended to produce large hail previously documented by MacGorman and Burgess (1994) and Stolzenburg (1994), and others having predominantly -CG and just account for small percentage of such storms. This tornadic supercell has predominantly -CG prior to hail-produce, switch to predominantly +CG when hail-produce (someone report hail produce at 1400, and dissipate time is unknown).

The enhancement for CG flash rate could be satisfying for the identification of severe weather, but unsatisfactory for the prediction of tornadoes.

## 5. Conclusions

The tornado distribution in China shows a major cluster over its plains. On such a plain, Jiangsu Province is low-lying, with extensive rivers and lakes. There is sufficient water vapor, which tends to focus energy from instability and foster severe convection. In the present work, based on the Yancheng EF4 tornado simulated by the WRF model, sounding data, and lightning detection network data, we found the following.

(1) The Yellow River and Huaihe regions have higher temperatures and greater humidity. There is a surface cyclone, rear inflow of cool air, and southwesterly jet stream at low levels. A low LCL, strong CAPE and vertical wind shear are favorable to the development of severe convective weather (e.g., supercells).

(2) Horizontal wind near the surface showed strong cyclonic shear when the EF4 tornado occurred. The simulated reflectivity revealed no hook echo but a weak echo region. A mesocyclone was the primary signature of a supercell storm, and there was cyclonic shear at various levels; a rotating updraft extended from mid to low levels of the cloud, indicative of mesocyclone formation.

(3) The observed and simulated +CG flash rates rose dramatically when hail was produced, respectively peaking 5 and 10 min afterward. The timing of simulated IC flash rates was consistent with that of +CG rates. The tornado occurred during a decrease of +CG flashes (its minimum 15 min earlier),

and the updraft volume peaked 5 min before tornado formation. The downdraft volume maximized upon tornadogenesis.

(4) During hail production to tornado formation, the charge structure mainly showed an inverted polarity charge structure, with several vertically stacked charge regions of alternating polarity. A mid-level strong positive charge, caused by positively charged graupel produced by a non-inductive charging mechanism, was moved to mid-levels by a strong updraft. A negative charge region formed because of an inductive charging mechanism and airflow beneath the strong positive charge region. Both charge regions had a dipole charge structure and most +CG flashes were initiated between low and mid-levels, owing to the strong potential between them. IC flashes were triggered between the mid and upper level charge regions. However, the lower negative charge region suppressed -CGs. Consequently, +CG flashes were dominant.

**Acknowledgements** Thank the National Centers for Environmental Prediction providing FNL reanalysis data. Thanks also go out to Dr. Mansell and Dr. Fierro from NOAA/OAR/NSSL in U.S. for putting forward some valuable suggestions about running WRF and adjusting parameterization scheme very much. Many thanks to Dr. Zheng from Chinese Academy of Meteorological Sciences for providing lightning data and Prof. Wei for providing SA radar data to compare simulated with observed. Special thanks go to Dr. Xie from Yunnan Meteorology Service in China for analyzing the synoptic background. This work was supported by the National Natural Science Foundation of China (Grant No. 41275008), the Basic Research Fund of the Chinese Academy of Meteorological Sciences (Grant No. 2016Z002), and the National Key Basic Research Program of China (Grant No. 2014CB441403).

## References

- Bluestein H B, MacGorman D R. 1998. Evolution of cloud-to-ground lightning characteristics and storm structure in the Spearman, Texas, tornadic supercells of 31 May 1990. *Mon Weather Rev*, 126: 1451–1467
- Branick M L, Doswell C A. 1992. An observation of the relationship between supercell structure and lightning ground-strike polarity. *Weather Forecast*, 7: 143–149
- Brooks H E, Doswell C A, Kay M P. 2003. Climatological estimates of local daily tornado probability for the United States. *Weather Forecast*, 18: 626–640
- Brooks I M, Saunders C P R. 1994. An experimental investigation of the inductive mechanism of thunderstorm electrification. *J Geophys Res*, 99: 10627–10632
- Browning K A. 1977. The structure and mechanisms of hailstorms. In: Foote G B, Knight C. *Hail: A Review of Hail Science and Hail Suppression*. Amer Meteorol Soc, 38: 1–47
- Carlson T N, Benjamin S G, Forbes G S, Li Y F. 1983. Elevated mixed layers in the regional severe storm environment: conceptual model and case studies. *Mon Weather Rev*, 111: 1453–1474
- Curran E B, Rust W D. 1992. Positive ground flashes produced by low-precipitation thunderstorms in Oklahoma on 26 April 1984. *Mon Weather Rev*, 120: 544–553
- Davies-Jones R P. 1982a. A new look at the vorticity equation with application to tornadogenesis. In: *Preprints 12 Conf. on Severe Local Storms*. San Antonio: Amer Meteorol Soc. 249–252
- Davies-Jones R P. 1982b. *Intense Atmospheric Vortices: Proceedings of the Joint Symposium: Observational and theoretical aspects of tornadogenesis*. Berlin: Springer. 175–189

- Davies-Jones R P. 2015. A review of supercell and tornado dynamics. *Atmos Res*, 158-159: 274–291
- Fan W J, Yu X D. 2015. Characteristics of spatial-temporal distribution of tornadoes in China (in Chinese). *Meteorol Month*, 41: 793–805
- Fierro A O, Mansell E R, MacGorman D R, Ziegler C L. 2013. The implementation of an explicit charging and discharge lightning scheme within the WRF-ARW Model: Benchmark simulations of a continental squall line, a tropical cyclone, and a winter storm. *Mon Weather Rev*, 141: 2390–2415
- Fujita T T. 1971. Proposed characterization of tornadoes and hurricanes by area and intensity. SMRP Research Paper vol. 91. Illinois: University of Chicago. 42
- Gilmore M S, Wicker L J. 2002. Influences of the local environment on supercell cloud-to-ground lightning, radar characteristics, and severe weather on 2 June 1995. *Mon Weather Rev*, 130: 2349–2372
- Guo F X, Lu G Y, Wu X, Wang H L, Liu Z P, Bao M, Li Y W. 2016. Occurrence conditions of positive cloud-to-ground flashes in severe thunderstorms. *Sci China Earth Sci*, 59: 1401–1413
- Houze R A, Smull B F, Dodge P. 1990. Mesoscale organization of springtime rainstorms in Oklahoma. *Mon Weather Rev*, 118: 613–654
- Kane R J. 1991. Correlating lightning to severe local storms in the Northeastern United States. *Weather Forecast*, 6: 3–12
- Kelly D L, Schaefer J T, McNulty R P, Doswell C A, Abbey R F. 1978. An augmented tornado climatology. *Mon Weather Rev*, 106: 1172–1183
- Lang T J, Rutledge S A. 2002. Relationships between convective storm kinematics, precipitation, and lightning. *Mon Weather Rev*, 130: 2492–2506
- Mansell E R, MacGorman D R, Ziegler C L, Straka J M. 2005. Charge structure and lightning sensitivity in a simulated multicell thunderstorm. *J Geophys Res*, 110: D12101
- Mansell E R, Ziegler C L, Bruning E C. 2010. Simulated electrification of a small thunderstorm with two-moment bulk microphysics. *J Atmos Sci*, 67: 171–194
- Markowski P M. 2002. Hook echoes and rear-flank downdrafts: A review. *Mon Weather Rev*, 130: 852–876
- McCaull E W, Goodman S J, LaCasse K M, Cecil D J. 2009. Forecasting lightning threat using cloud-resolving model simulations. *Weather Forecast*, 24: 709–729
- MacGorman D R, Rust W D, Mazur V. 1985. Lightning activity and mesocyclone evolution 17 May 1981. In: Preprints 14th Conf. on Severe Local Storms. Indianapolis: Amer Meteorol Soc. 355–358
- MacGorman D R, Burgess D W. 1994. Positive cloud-to-ground lightning in tornadic storms and hailstorms. *Mon Weather Rev*, 122: 1671–1697
- MacGorman D R, Burgess D W, Mazur V, Rust W D, Taylor W L, Johnson B C. 1989. Lightning rates relative to tornadic storm evolution on 22 May 1981. *J Atmos Sci*, 46: 221–251
- MacGorman D R, Nielsen K E. 1991. Cloud-to-ground lightning in a tornadic storm on 8 May 1986. *Mon Weather Rev*, 119: 1557–1574
- MacGorman D R, Straka J M, Ziegler C L. 2001. A Lightning parameterization for numerical cloud models. *J Appl Meteorol*, 40: 459–478
- MacGorman D R, Rust W D, Krehbiel P, Rison W, Bruning E, Wiens K. 2005. The electrical structure of two supercell storms during STEPS. *Mon Weather Rev*, 133: 2583–2607
- Moller A R, Doswell C A, Przybylinski R. 1990. High-precipitation supercells: A conceptual model and documentation. In: Preprints, 16th Conf. on Severe Local Storms. Kananaskis: Amer Meteorol Soc. 52–57
- Moller A R, Doswell C A, Foster M P, Woodall G R. 1994. The operational recognition of supercell thunderstorm environments and storm structures. *Weather Forecast*, 9: 327–347
- Pan W Z. 2008. Studies on the distribution characteristics and hazard evaluation of tornadoes in Jiangsu (in Chinese). Dissertation for Doctoral Degree. Nanjing: Nanjing University of Information Science and Technology
- Perez A H, Wicker L J, Orville R E. 1997. Characteristics of cloud-to-ground lightning associated with violent tornadoes. *Weather Forecast*, 12: 428–437
- Rust W D, MacGorman D R, Bruning E C, Weiss S A, Krehbiel P R, Thomas R J, Rison W, Hamlin T, Harlin J. 2005. Inverted-polarity electrical structures in thunderstorms in the severe thunderstorm electrification and precipitation study (STEPS). *Atmos Res*, 76: 247–271
- Reap R M, MacGorman D R. 1989. Cloud-to-ground lightning: Climatological characteristics and relationships to model fields, radar observations, and severe local storms. *Mon Weather Rev*, 117: 518–535
- Saunders C P R, Peck S L. 1998. Laboratory studies of the influence of the rime accretion rate on charge transfer during crystal/graupe collisions. *J Geophys Res*, 103: 13949–13956
- Stolzenburg M. 1994. Observations of high ground flash densities of positive lightning in summertime thunderstorms. *Mon Weather Rev*, 122: 1740–1750
- Tan Y B, Chen C, Zhou J C, Zhou B W, Zhang D D, Guo X F. 2016. A parameterization scheme for upward lightning in the cloud model and a discussion of the initial favorable environmental characteristics in the cloud. *Sci China Earth Sci*, 59: 1440–1453
- Weisman M L, Klemp J B. 1984. The structure and classification of numerically simulated convective storms in directionally varying wind shears. *Mon Weather Rev*, 112: 2479–2498
- Wicker L J, Williamson R B. 1995. Simulation and analysis of tornado development and decay within a three-dimensional supercell thunderstorm. *J Atmos Sci*, 52: 2675–2703
- Williams E R. 2001. The electrification of severe storms. *Meteorol Monographs*, 28: 527–528
- Wines K C, Rutledge S A, Tessendorf S A. 2005. The 29 June 2000 supercell observed during STEPS. Part II: Lightning and charge structure. *J Atmos Sci*, 62: 4151–4177
- Witt A, Eilts M D, Stumpf G J, Johnson J T, Mitchell E D W, Thomas K W. 1988. An enhanced hail detection algorithm for the WSR-88D. *Weather Forecast*, 13: 286–303
- Yao Y Q, Yu X D, Zhang Y J, Zhou Z J, Xie W S, Lu Y Y, Yu J L, Wei L X. 2015. Climate analysis of tornadoes in China. *J Meteorol Res*, 29: 359–369
- Zhang Y, Krehbiel P R, Hamlin T, Thomas R J, Rison W. 2001. Electrical charge structure and cloud-to-ground lightning in thunderstorms during STEPS. In: Amer Geophys Union, Fall Meeting 2001. Abstract #AE12A-0079
- Zheng Y Y, Zhu H F, Fang X, Zhang X C, Xue C, Yao C, Hao Y. 2009. Characteristic analysis and early-warning of tornado supercell storm (in Chinese). *Plateau Meteorol*, 3: 617–625